

Article

Numerical Simulation of CO₂-ECBM Based on Multi-Physical Field Coupling Model

Ziwen Li , Hongjin Yu * and Yansong Bai

College of Safety and Emergency Management Engineering, Taiyuan University of Technology, Taiyuan 030024, China
* Correspondence: yuhongjin1569@link.tyut.edu.cn; Tel.: +86-157-3521-9759

Abstract: In this paper, heat injection and CO₂ injection are combined, and the influence of coal seam parameters on CO₂-ECBM is analyzed to improve the production of CH₄ and CO₂ reserves and the effective control of both greenhouse gases. A multi-physical field coupling model of CO₂-ECBM was established based on Darcy's law, Fick's law of diffusion, the extended Langmuir model for adsorption, and the equation of state. Numerical simulation of CO₂-ECBM under different coal seam parameters was carried out by COMSOL Multiphysics. The results show that increasing the injection pressure of the CO₂ injection well and the initial pressure of the coal seam can effectively increase the gas pressure and concentration gradient, which has a positive effect on improving the extraction concentration of CH₄ and the sequestration concentration of CO₂ in the coal seam. The increase of the initial temperature of the coal seam will promote the desorption and diffusion of the binary elemental gas, resulting in a decrease in the concentration of coalbed methane and a decrease in the displacement effect. In the process of displacement, the greater the initial permeability, the greater the fracture opening of the coal seam, which is more conducive to the seepage transport of the gas. The closer to the position of the injection well, the better the displacement effect and the lower the permeability rate ratio.

Keywords: CO₂-ECBM; multi-physical field coupling; CO₂ and CH₄ concentration; permeability; displacement effect



Citation: Li, Z.; Yu, H.; Bai, Y. Numerical Simulation of CO₂-ECBM Based on Multi-Physical Field Coupling Model. *Sustainability* **2022**, *14*, 11789. <https://doi.org/10.3390/su141811789>

Academic Editors: Wei Yang, He Li and Ting Liu

Received: 1 September 2022

Accepted: 17 September 2022

Published: 19 September 2022

Publisher's Note: MDPI stays neutral with regard to jurisdictional claims in published maps and institutional affiliations.



Copyright: © 2022 by the authors. Licensee MDPI, Basel, Switzerland. This article is an open access article distributed under the terms and conditions of the Creative Commons Attribution (CC BY) license (<https://creativecommons.org/licenses/by/4.0/>).

1. Introduction

With the development of modern industrial technology, humans use a large amount of fossil energy, and CO₂ emissions have increased significantly. Therefore, the “greenhouse effect” has become a globally significant issue. In the process of coal mining, coalbed methane (CBM), a highly efficient, non-polluting flammable gas, is released from coal seams. Meanwhile, CBM is the greenhouse gas second only to CO₂, and its direct emission into the atmosphere will not only cause air pollution but also cause a huge waste of resources [1,2]. Due to the high gas storage capacity of coal, CH₄ recovery and CO₂ storage have received attention in many countries [3,4]. The technology of injecting CO₂ into coal seams to improve the CH₄ extraction rate (hereinafter referred to as CO₂-ECBM) can not only reduce greenhouse gas emission but also develop new energy, which has attracted widespread attention [5,6]. CO₂-ECBM not only addresses safety issues, increasing environmental requirements, but also extracts methane from coal for additional energy use [7]. CO₂-ECBM is mainly based on competitive adsorption between CH₄ and CO₂. With the injection of CO₂, the affinity of CO₂ on coal is greater than that of CH₄; for every CH₄ molecule released, at least two CO₂ molecules can be absorbed [8,9]. Therefore, CO₂ begins to occupy the adsorption sites of CH₄ [10], and this will decrease the harmful influences of carbon dioxide gas on the existing climate by providing safe storage locations. Moreover, the method of ECBM recovery by injecting flue gas into the coal seams may be a striking alternative way of increasing the production of gas considerably [11]. Therefore, it is of great significance

to improve CO₂-ECBM by establishing a reasonable and accurate mathematical model to simulate CBM exploitation and compare different coal seam parameters.

For the CO₂-ECBM, many countries have carried out pilot experimental research and proved the feasibility, economic and environmental benefits of this project. Among them, numerical simulation research is one of the main research directions of gas injection displacement. It can quantitatively analyze the potential of CO₂-ECBM, and the research investment is small and the time involved is short [12]. Multiphysics coupling numerical simulation research has been widely used in the field of CBM development [13], and some experimental studies have been carried out at home and abroad to prove the feasibility of this project. Fang et al. [14] established a fluid-solid coupling model of CO₂-ECBM to study the distribution of gas pressure and concentration, and analyzed the CH₄ production and CO₂ storage, but ignored the effect of thermal field on displacement, and only the coupling of force field and mechanical field is carried out. Qu et al. [15] established a permeability evolution model in CO₂-ECBM which only considered a single gas and ignored the effect of competitive adsorption between multiple gases. Perera [16] used COMET3 to establish a three-dimensional numerical model for the numerical simulation of CO₂-ECBM, only considering the effect of temperature changes on the coal skeleton strain. Yang et al. [17] established a multi-physics coupled mathematical model to simulate the variation of borehole gas discharge flow and drain flow when N₂ and CO₂ were injected into the coal seam, but ignored the influence of thermal fields on multi-physics fields. Rutqvist et al. [18] proposed a thermal-water-mechanical coupling model to analyze the multiphase fluid flow, heat transfer and deformation in porous and fractured rocks, although the disadvantage is that the influence of gas adsorption and the Klinkenberg effect on the whole is not considered. Sun [19] established multi-component gas flow models for coalbed CO₂ injection and CH₄ exploitation, but these models did not consider the fluid-solid coupling effect of coal seams.

From the above analysis it can be seen that the injection of heat into the coal seam and the injection of CO₂ into the coal seam can both affect the effect of CBM extraction. However, few studies have been published on combining heat injection and CO₂ injection to reduce CH₄ concentration in coal seams. In order to be closer to the actual geological conditions, the typical three-wells layout of the CO₂-ECBM project in the Qinshui basin is selected as the research object. The depth of coal seam is 1200–2000 m; the No. 3 coal seam is mainly the primary structure coal, the macro coal and rock composition are mainly bright coal, with mirror coal strip, and the micro coal and rock composition is mainly vitrinite, The content ranged from 74.9% to 77.9%, with an average of 76.4%. The inertinite content was 22.4–25.1%, with an average of 23.18%. The mineral content ranged from 16.0% to 22.5%, with an average of 19.2%. The maximum reflectance of vitrinite is 2.2–3.0%, which is mainly anthracite. The ash content of the coal seam is 8–15%, which is from the low ash coal [20].

In this work, the fluid-solid-thermal coupling model of CO₂-ECBM was established, consider the permeation, diffusion and competitive adsorption of binary gas in the coal seam, the influence of coal seam initial temperature on CO₂-ECBM is studied, permeability evolution and displacement effect in the reservoir under different CO₂ injection pressures and initial coal seam pressures were analyzed. The influence of the different initial permeability of the coal seam on the displacement effect was also discussed. Based on the COMSOL Multiphysics numerical simulation software, the influence of different characteristic parameters on the displacement effect was analyzed by comparing the displacement effect under different coal seam parameters; the CO₂ extraction and CH₄ storage can be improved, the greenhouse gas content can be effectively reduced and more clean energy can be obtained. This provided the basis for the prediction of the CO₂-ECBM and the engineering site selection.

2. Materials and Methods

2.1. Model Assumptions

The injection of CO₂ to displace CH₄ in coal seams is a complex multiphase flow coupled process. The displacement process is often accompanied by multi-physical field coupling effects such as gas adsorption and desorption, coal seam deformation, and the heat exchange of the gas and coal skeleton. In order to explore the mechanism of multi-physical field coupling in the process of CO₂-ECBM, the following assumptions need to be made [21–23]: ① The coal seam is a homogeneous isotropic body, and the gas is evenly distributed in the coal seam; ② The deformation of the coal seam is an infinitesimal deformation; ③ The gas in the coal seam is an ideal gas, and the influence of temperature change on the gas dynamic viscosity is not considered; ④ The seepage and diffusion of CH₄ and CO₂ conform to Darcy's law and Fick's law, respectively; and ⑤ The influence of water and vapor on gas transport is not considered [24].

2.2. Gas Transport Equation

According to the assumption, CBM is first in a dynamic equilibrium state of adsorption and desorption. When the equilibrium state is broken due to the injection of CO₂, the CH₄ in the adsorbed state is desorbed and diffused into the fracture system under the action of the concentration gradient. The equation describing this phenomenon can be expressed as [13,25,26]:

$$\frac{\partial m_n}{\partial t} + \nabla \cdot (\vec{v} \cdot \rho_{gn}) + \nabla \cdot (-\vec{D}_n \cdot \nabla m_{fn}) = Q_{sn}. \quad (1)$$

In the formula, m_n is the gas content, including free phase gas and adsorbed gas, kg/m³; n is the gas code, n is 1 for CH₄, n is 2 for CO₂; t is time, s; ∇ is the Laplace calculation; m_{fn} is the mass of the free phase gas, kg/m³; m_{sn} is the mass of the adsorbed gas, kg/m³; \vec{v} is the convection velocity vector; ρ_{gn} is the gas density, kg/m³; Q_{sn} is the source term W/m³.

$$Q_{sn} = -(1 - \phi_0) \cdot \rho_c \cdot \rho_{sg} \cdot DD \cdot \frac{\partial C_n}{\partial t}. \quad (2)$$

where:

$$DD = \frac{V_{ljo} \exp\left[-\frac{d_2(T-T_0)}{1+d_1 C_n RT}\right] \cdot C_n \cdot b_1 \cdot b_2 \cdot (R \cdot T)^2}{(1 + C_1 \cdot b_1 RT + C_2 \cdot b_2 RT)^2}.$$

The mass of gas contained in a unit volume of coal can be defined as [27]:

$$m_n = m_{fn} + m_{sn} = \phi \cdot C_n \cdot M_n + (1 - \phi) \cdot \rho_c \cdot \rho_{sg} \frac{V_{\infty n} b_n C_n}{1 + C_1 b_1 + C_2 b_2}. \quad (3)$$

In the formula: ϕ is the porosity of coal seam; ρ_c is the coal density, kg/m³; $V_{\infty n}$ is the corrected Langmuir volume constant, m³/kg; ρ_{sg} is the gas density at standard conditions, kg/m³; M_n is the molar mass of the component, k; C_n is the gas concentration, mol/m³; b_n is the Langmuir pressure constant, Pa⁻¹.

Where: \vec{v} is the convective velocity vector, which is determined by the injection gas concentration gradient and can be expressed as [27]:

$$\vec{v} = -\frac{kRT}{\mu} \nabla C_n. \quad (4)$$

Substitute Equations(2), (3) and (4) into Equation (1) to obtain the gas migration formula in the coal seam:

$$\left[\phi \cdot M_n + (1 - \phi) \cdot \rho_c \cdot P_{sg} \cdot AA\right] \cdot \frac{\partial C_n}{\partial t} + \nabla \cdot \left(-C_n \cdot \frac{k \cdot R \cdot T}{\mu_n} \nabla C_n\right) + \nabla \cdot (-D_n \cdot \phi \nabla C_n) = Q_{sn}. \quad (5)$$

where:

$$AA = \frac{V_{\infty n} \cdot b_n \cdot R \cdot T (1 + C_n \cdot b_n \cdot R \cdot T)}{(1 + C_1 \cdot b_1 \cdot RT + C_2 \cdot b_2 \cdot RT)^2}.$$

where: k is the permeability of the coal seam, m^2 ; R is the gas molar constant, $\frac{J}{mol \cdot K}$; T is the coal seam temperature, K ; μ_n is the dynamic viscosity coefficient of the gas, $Pa \cdot s$; M_n is the mole of the gas mass, $\frac{kg}{mol}$; D_n is the vector of hydrodynamic dispersion coefficient.

2.3. Governing Equation of Coal Seam Stress Field

Gas transport and exchange typically causes significant changes in effective stress, so that influences coal seam deformation and the evolution of transport parameters.

The Navier equation of the force balance of the CH₄-containing coal seam is [28,29]:

$$\sigma_{ij,i} + f_i = 0. \quad (6)$$

In the formula, $\sigma_{ij,i}$ is the stress tensor; f_i is the body force component, and this study only considers the vertical gravity.

Considering that the elastic deformation of coal seam is small deformation, the strain-displacement relation is defined as [28,30]:

$$\varepsilon_{i,j} = \frac{1}{2}(u_{i,j} + u_{j,i}). \quad (7)$$

The constitutive equation for the deformed coal seam becomes [28,30]:

$$\varepsilon_{ij} = \frac{1}{2G}\sigma_{ij} - \left(\frac{1}{6G} - \frac{1}{9K}\right)\sigma_{KK}\delta_{ij} + \frac{\alpha}{3k}p\delta_{ij} + \frac{\varepsilon_s}{3}\delta_{ij}. \quad (8)$$

In the formula: $G = \frac{E}{2(1+\nu)}$, $K = \frac{E}{3(1-2\nu)}$; K , K_s are the bulk modulus of coal and coal grains respectively, Pa ; G is the shear modulus of coal, Pa ; E is the Young's modulus of the coal; ν is the Poisson's ratio of the coal; δ_{ij} is the Kronecker delta.

$$Gu_{i,jj} + \frac{G}{1-2\nu}u_{j,ji} = (\alpha \cdot RT + K \cdot BB)C_{1,i} + (\alpha \cdot RT + K \cdot CC)C_{2,i} - K \cdot \alpha_T T_i - f_i. \quad (9)$$

where: $BB = \frac{\varepsilon_{\infty 1} b_1 (1+b_2 C_2)}{(1+b_1 C_1 + b_2 C_2)^2} - \frac{\varepsilon_{\infty 2} b_1 b_2 C_2}{(1+b_1 C_1 + b_2 C_2)^2}$; $CC = \frac{\varepsilon_{\infty 2} b_2 (1+b_1 C_1)}{(1+b_1 C_1 + b_2 C_2)^2} - \frac{\varepsilon_{\infty 1} b_1 b_2 C_1}{(1+b_1 C_1 + b_2 C_2)^2}$; $\varepsilon_{\infty n}$ is the gas swelling strain constant.

2.4. Control Equation of Coal Seam Temperature Field

In the entire fluid-solid-thermal coupled model, the coal seam temperature changes are mainly caused by the exothermic or endothermic reactions induced by CO₂ injection and adsorption-desorption during the displacement process. Based on the energy conservation law and the Fourier law, the control equation of the coal seam temperature field can be obtained [31–33]:

$$\frac{\partial((\rho C_p)_c T)}{\partial t} + \eta \nabla T - \nabla \cdot (\lambda_c \nabla T) + q_{st1} \frac{\rho_C \rho_{sg1}}{M_1} \frac{\partial V_{c1}}{\partial t} + q_{st2} \frac{\rho_C \rho_{sg2}}{M_2} \frac{\partial V_{c2}}{\partial t} + K \alpha_T T \frac{\partial(\varepsilon_{s1} + \varepsilon_{s2})}{\partial t} = 0. \quad (10)$$

In the formula: $(\rho C_p)_c$ is the effective heat capacity, $\frac{J}{m^3 \cdot K}$; η is the convection coefficient, $\frac{J}{m^2 \cdot s}$; λ_c is the effective coefficient of the isotropic thermal conductivity, $\frac{W}{m \cdot K}$; q_{st1} is the isosteric heat of adsorption of CH₄, $\frac{J}{mol}$; ρ_{sg1} is the gas density of CH₄ under standard conditions, $\frac{kg}{m^3}$; V_{c1} is the mass of CH₄ adsorbed by coal, $\frac{m^3}{m^3}$; q_{st2} is CO₂ isosteric heat of adsorption, $\frac{J}{mol}$; ρ_{sg2} is CO₂ gas density under standard conditions, $\frac{kg}{m^3}$; V_{c2} is the mass of CO₂ adsorbed by the expansion and shrinkage of the matrix, $\frac{m^3}{m^3}$; ε_{s1} is the total volume

strain generated by the adsorption or desorption of CH₄ by the coal; ε_{s2} is the total volume strain generated by the adsorption or desorption of CO₂ by the coal;

$$(\rho C_p)_c = (1 - \phi)\rho_c C_s + \phi(M_1 C_{v1} C_{L1} + M_2 C_{v2} C_{L1}). \quad (11)$$

$$\eta = -\frac{k}{\mu_1} \nabla C_1 RT \rho_{ga1} C_{L1} - \frac{k}{\mu_2} \nabla C_2 RT \rho_{ga2} C_{L2}. \quad (12)$$

$$\lambda_c = (1 - \phi)\lambda_s + \phi(\lambda_{g1} + \lambda_{g2}). \quad (13)$$

where: ϕ is the porosity; C_{v1} is the volume fraction of CH₄ in coal seam; C_{L1} is the constant volume specific heat capacity of CH₄, $\frac{J}{m^3 \cdot K}$; C_{v2} is the volume fraction of CO₂ s in the coal seam; C_{L2} is the constant volume specific heat capacity of CO₂, $\frac{J}{m^3 \cdot K}$; λ_{g1} is the heat conductivity coefficient of the coal skeleton of CH₄, $\frac{W}{m \cdot K}$; λ_{g2} is the heat conductivity coefficient of the coal skeleton of CO₂, $\frac{W}{m \cdot K}$.

2.5. Coupling Terms

After gas injection, there are only CO₂ and CH₄ in the coal seam. The calculation formula of the total gas adsorption is as follows [34,35]:

$$V = V_{CO_2} + V_{CH_4} = \frac{V_{L1} b_1 P_1 + V_{L2} b_2 P_2}{1 + b_1 P_1 + b_2 P_2}. \quad (14)$$

where: V_{L1} and V_{L2} are the Langmuir volume constants of CH₄ and CO₂, respectively, $\frac{m^3}{kg}$; P_1 and P_2 are the partial pressures of CH₄ and CO₂, respectively, MPa.

Binary gas adsorption and desorption can cause stress deformation of the coal seam, and the calculation formula of the total volume strain is [36]:

$$\varepsilon_s = \varepsilon_{CO_2} + \varepsilon_{CH_4} = \frac{\varepsilon_{L1} b_1 P_1 + \varepsilon_{L2} b_2 P_2}{1 + b_1 P_1 + b_2 P_2}. \quad (15)$$

where ε_{L1} and ε_{L2} are the Langmuir volume strain constants of CH₄ and CO₂, respectively.

By analyzing the coupled model, the porosity model is obtained [34]:

$$\phi = \frac{V_p}{V} = 1 - \frac{1 - \phi_0}{1 + \varepsilon_V} \left(1 + \frac{\Delta V_s}{V_{s0}} \right). \quad (16)$$

where: V_p is the pore volume of coal, m³; V is the total volume of coal, m³; ϕ_0 is the initial porosity; ε_V is the volumetric strain of coal seam; ΔV_s is the change of skeleton volume, m³; V_{s0} is the initial skeleton volume, m³.

$$\frac{\Delta V_s}{V_{s0}} = -\frac{\alpha}{K_s} (\Delta P_1 + \Delta P_2) + \Delta \varepsilon_s + \alpha_s \cdot \Delta T. \quad (17)$$

α is the Biot effective stress coefficient; K_s is the volume modulus of the skeleton, MPa; α_s is the thermal expansion coefficient, K⁻¹; T is the temperature, K.

Which brings (17) into (16):

$$\phi = \frac{V_p}{V} = 1 - \frac{1 - \phi_0}{1 + \varepsilon_V} \left[1 - \frac{\alpha}{K_s} (\Delta P_1 + \Delta P_2) + \Delta \varepsilon_s + \alpha_s \cdot \Delta T \right]. \quad (18)$$

The model is [37,38]:

$$k = k_0 \left[\frac{1}{\phi_0} - \frac{1 - \phi_0}{\phi_0 (1 + \varepsilon_V)} \left(1 - \frac{\alpha}{K_s} (\Delta P_1 + \Delta P_2) + \Delta \varepsilon_s + \alpha_s \cdot \Delta T \right) \right]^3. \quad (19)$$

In the formula: k_0 is the initial permeability, m².

2.6. Fluid-Solid-Thermal Field Cross-Coupling

Governing equations and coupling terms are nonlinear second-order partial differential equations (PDEs) in space and time domains. Therefore, we introduced these equations into the solid mechanics and PDE module of COMSOL Multiphysics (COMSOL Multiphysics 5.6) to obtain numerical solutions through discrete and finite element methods. The coupling effect of CBM mining can be obtained by combining Equations (18) and (19), combining Equations (5), (9) and (10) the THM coupled mathematical model can be achieved, see the following equation.

It can be seen from the above formula that each physical field is coupled and related to each other, and the relationship between them is shown in Figure 1. The temperature stress caused by the change of temperature has an impact on the mechanic model; the strain energy generated by energy dissipation within the skeleton has an impact on the coal seam temperature; the change of temperature causes the change of gas adsorption and desorption, which has an impact on the gas transport model; the heat transfer and the seepage of gas has an impact on the temperature model; the change of porosity and permeability caused by coal deformation has an impact on the gas transport model; and the change of gas pressure can result in coal deformation.

Governing equation	{	Gas transport model: $[\phi \cdot M_n + (1 - \phi) \cdot \rho_c \cdot P_{sg} \cdot AA] \cdot \frac{\partial C_n}{\partial t} + \nabla \left(-C_n \cdot \frac{k \cdot R \cdot T}{\mu_n} \nabla C_n \right) + \nabla (-D_n \cdot \phi \nabla C_n) = Q_{sn}.$
		Mechanical model: $Gu_{i,jj} + \frac{G}{1-2\nu} u_{j,ji} = (\alpha \cdot RT + K \cdot BB)C_{1,i} + (\alpha \cdot RT + K \cdot CC)C_{2,i} - K \cdot \alpha_T T_{,i} - f_i.$
		Temperature field: $\frac{\partial((\rho c_p)_c T)}{\partial t} + \eta \nabla T - \nabla \cdot (\lambda_c \nabla T) + q_{st1} \frac{\rho c p_{sg1}}{M_1} \frac{\partial V_{c1}}{\partial t} + q_{st2} \frac{\rho c p_{sg2}}{M_2} \frac{\partial V_{c2}}{\partial t} + K \alpha_T T \frac{\partial(\varepsilon_{s1} + \varepsilon_{s2})}{\partial t} = 0.$
Coupling terms	{	Permeability: $k = k_0 \left[\frac{1}{\phi_0} - \frac{1 - \phi_0}{\phi_0(1 + \varepsilon_V)} \right] \left(1 - \frac{\alpha}{K_S} (\Delta P_1 + \Delta P_2) + \Delta \varepsilon_s + \alpha_s \cdot \Delta T \right)^3.$
		Porosity: $\phi = \frac{V_P}{V} = 1 - \frac{1 - \phi_0}{1 + \varepsilon_V} \left[1 - \frac{\alpha}{K_S} (\Delta P_1 + \Delta P_2) + \Delta \varepsilon_s + \alpha_s \cdot \Delta T \right].$

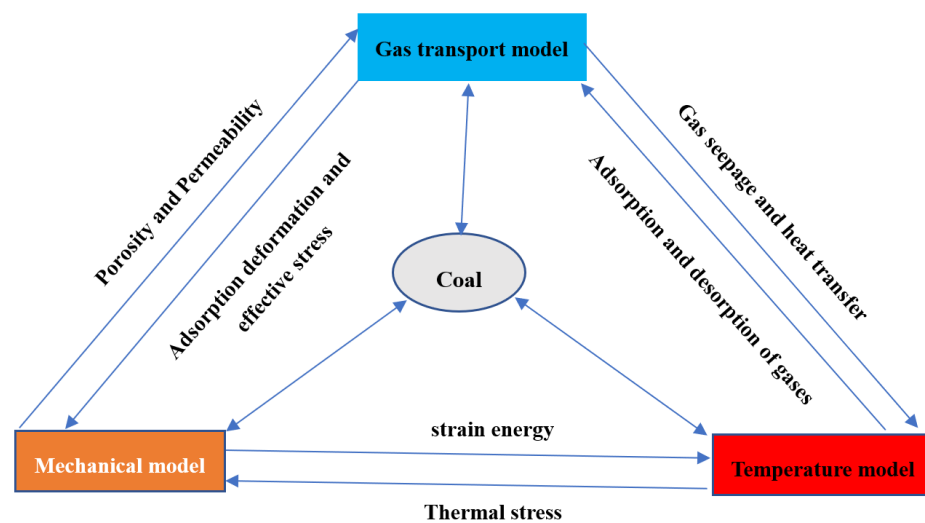


Figure 1. The coupling relationships among the multi-physics fields during the CO₂-ECBM.

2.7. Geometric Model Description

Qinshui Basin is located in the south-central Shanxi province; it is one of the most active and promising areas for CBM exploration and development in China. The No. 3 coal seam in the Qinshui basin is the main target area because of its unique characteristics, such as stable tectonic environment, weak hydrodynamic condition and good regional cap [32].

The CO₂-ECBM is actually a 3D model, but compared with the parallel bedding direction, the coal seam perpendicular to the bedding direction can be ignored. It can be approximated as a 2D model. The model diagram is shown in Figure 2. The model selects a square area of 150 m × 150 m as the research domain, with a radius of 0.1 m. The W_{in} , CO₂ injection well is located at the lower left corner of the geological model, and the W_{out} , CH₄ production well is located at the upper right corner of the model. Observation point A is selected to observe the simulation effect, and points B and C are the comparison points.

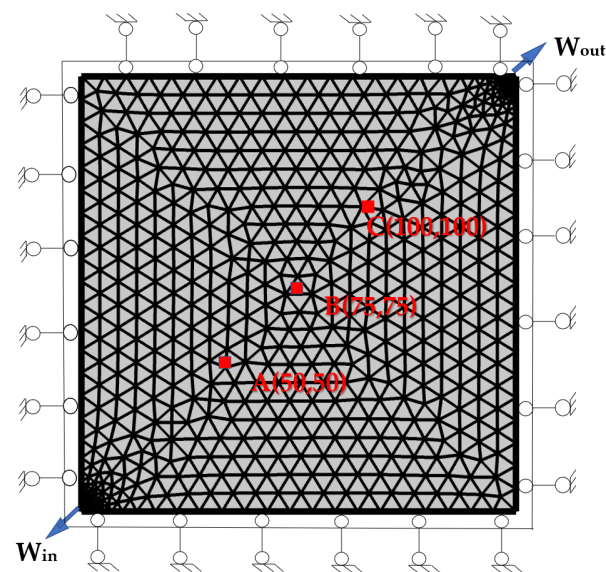


Figure 2. Schematic of the simulation model.

3. Results and Discussion

3.1. Boundary Conditions

Except for the boundary of the injection well and the production well, the other boundaries have zero flow boundary conditions with no outflow and no heat conduction. The average thickness of the coal seam is 5 m, the initial gas pressure is 5 MPa, the CO₂ injection well pressure is set to 8 MPa, the initial permeability is $5.14 \times 10^{-16} \text{m}^2$, the injection wellbore are constant temperature boundary conditions of 300 K, and the initial coal seam temperature is 300 K. Other parameters used in the numerical simulations are taken from the literature and are listed in Table 1. [25,30–32].

Table 1. Numerical simulation parameters.

Parameter	Numerical Value	Parameter	Numerical Value
Young's modulus of coal E/MPa	2710	Coal skeleton expansion coefficient α_T / K^{-1}	$2.4 \cdot 10^{-5}$
Poisson's ratio of coal ν	0.35	CO ₂ specific heat capacity $C_s / [\text{J}/(\text{kg} \cdot \text{K})]$	1250
Density of coal $\rho_s / (\text{kg}/\text{m}^3)$	1370	CO ₂ thermal conductivity $\lambda_{ge} / [\text{W}/(\text{m} \cdot \text{K})]$	0.015
Initial porosity of coal ϕ_0	0.037	CO ₂ constant pressure heat capacity $C_{pe} / [\text{J}/(\text{mol} \cdot \text{K})]$	37.18

Table 1. Cont.

Parameter	Numerical Value	Parameter	Numerical Value
Dynamic viscosity coefficient of CH ₄ $\mu_1/(\text{Pa}\cdot\text{s})$	1.84×10^{-5}	Dynamic viscosity coefficient of CO ₂ $\mu_2/(\text{Pa}\cdot\text{s})$	1.84×10^{-5}
Skeletal Young's Modulus E_s/MPa	8469	CH ₄ thermal conductivity $\lambda_{g1}/[\text{W}/(\text{m}\cdot\text{K})]$	0.031
CH ₄ heat capacity at constant pressure $C_{pj}/[\text{J}/(\text{mol}\cdot\text{K})]$	34.4	Thermal conductivity of coal skeleton $\lambda_s/[\text{W}/(\text{m}\cdot\text{K})]$	0.191
CH ₄ Langmuir pressure P_{l10}/MPa	2.07	CO ₂ Langmuir pressure P_{l20}/MPa	1.38
CH ₄ Langmuir volume $V_{l10}/(\text{m}^3/\text{kg})$	0.0256	CO ₂ Langmuir volume $V_{l20}/(\text{m}^3/\text{kg})$	0.0477
CH ₄ dynamic dispersion coefficient $D_1/(\text{m}^2/\text{s})$	3.6×10^{-12}	CO ₂ dynamic dispersion coefficient $D_2/(\text{m}^2/\text{s})$	5.8×10^{-12}
Coal skeleton density $\rho_s/(\text{g}/\text{m}^3)$	1470	CO ₂ isosteric heat of adsorption $q_{st2}/(\text{J}/\text{mol})$	33.4
CH ₄ isosteric heat of adsorption $q_{st1}/(\text{J}/\text{mol})$	35	Temperature correction coefficient d_2/K^{-1}	0.021
Pressure correction coefficient d_1/K^{-1}	0.071		

3.2. CBM Extraction Law

3.2.1. Pressure Cloud Map Distribution

In the process of CO₂-ECBM, with the continuous injection of CO₂ and the continuous extraction of CH₄, the concentrations of CO₂ and CH₄ and pore pressure of the coal seam will also change continuously. Figure 3 shows the cloud map distribution.

It can be seen from Figure 2a,b that with the continuous injection of CO₂, CO₂ enters the coal seam from the injection well in the lower left corner and diffuses throughout the coal seam. When the gas injection time is 100 days, the influence radius is only 50 m. By 3650 days, the influence radius has reached about 170 m. Figure 3c,d show the CH₄ concentration distribution as CH₄ is pumped out from the upper right production well. It can be seen from the figures that the CH₄ concentration has been effectively reduced. At 100 days, the CH₄ concentration was 1971.916 mol/m³, and at 3650 days, the CH₄ concentration was 1102.834 mol/m³, which is a decrease of 44%.

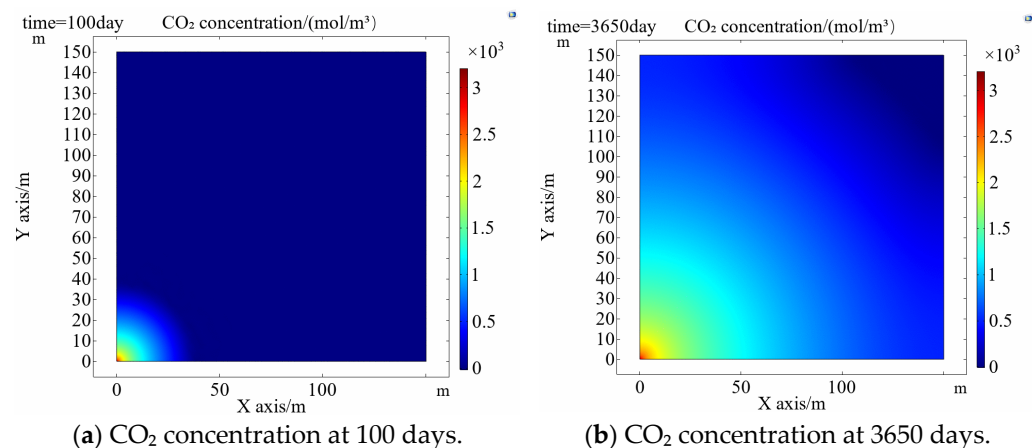


Figure 3. Cont.

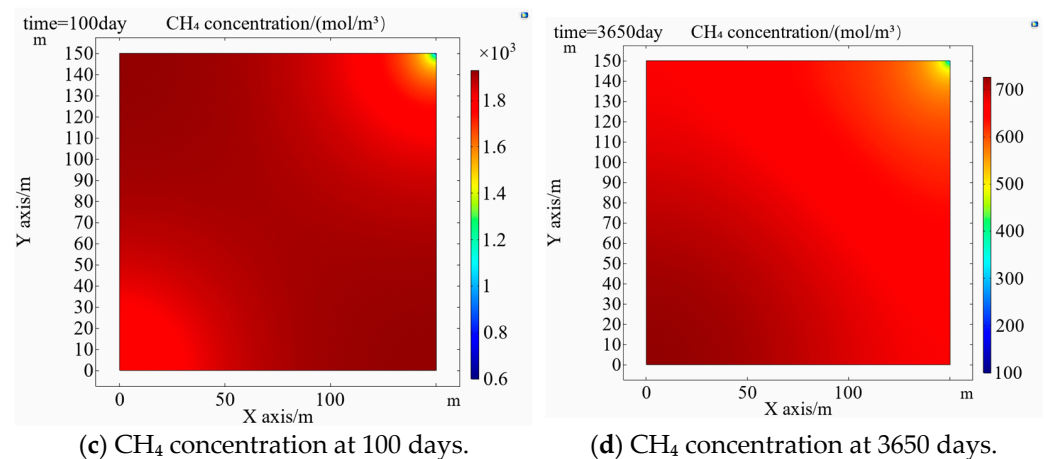


Figure 3. Distribution of CO₂ and CH₄ concentrations in coal seams.

3.2.2. Displacement Effect at Different Positions of Coal Seam

The displacement effect at different positions of the coal seam is shown in Figure 4, where the positions of point A, B and C are (50, 50), (75, 75), (100, 100) respectively. It can be seen from the figure that the closer to the injection well, the better the displacement effect. The change of coal seam permeability is the result of the combined action of the multi-physical field. When these three points are not affected by CO₂, the permeability ratio is a process of slightly decreasing and then increasing. The larger initial permeability corresponds to higher gas velocity [22]. This is because CH₄ flows out of the CH₄ production well, causing the pressure to decrease. The CH₄ pressure decreases over time, and the increase in effective stress reduces the pore size of the fracture and its space, resulting in a decrease in permeability. When CH₄ is desorbed from the coal seam, the coal seam shrinks, which leads to an increase in the fracture space, and the increase of the fracture caused by desorption is much greater than the decrease of the fracture space caused by the increase of effective stress, so the permeability gradually increases with time [14,29].

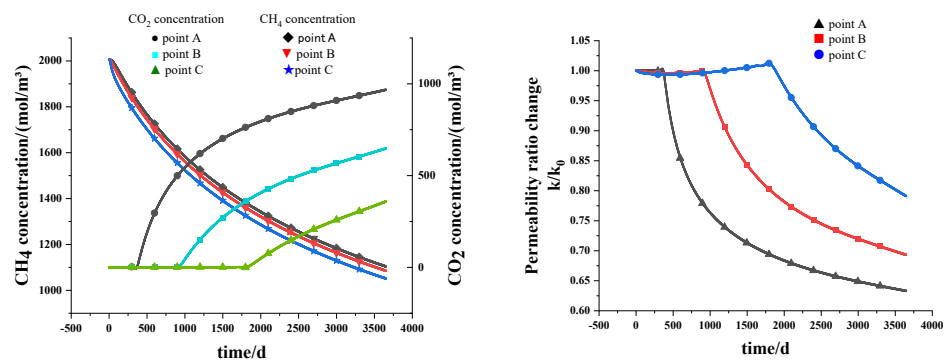


Figure 4. Displacement effect at different positions of coal seam.

Point A, B and C have different distances from the CO₂ injection well. The farther the distance is, the longer the CO₂ injection was unaffected. As time increases, CO₂ injection affects points A, B and C, while CO₂ injection causes matrix shrinkage [14], and the permeability ratio decreases. This is because the closer to the injection well, the higher the CO₂ concentration, which leads to an increase in the amount of CO₂ adsorption under the competitive adsorption, the greater the space expansion of the coal seam, and lower permeability. The farther the distance from the CO₂ injection well, the lower the CO₂ concentration at this point, the smaller the pressure gradient formed, and the slower the seepage velocity, the less chance for CO₂ to contact CH₄, and the worse the displacement

effect [34]. Therefore, the displacement effect of point A is greater than that of point B, and the displacement effect of point B is greater than that of point C.

3.3. Influence of Coal Seam Characteristic Parameters on CO₂-ECBM

3.3.1. Displacement Effect under Different Initial Temperatures

Figure 5 shows the displacement effect of different initial temperatures at point A within 3650 d. With the injection of CO₂, the permeability decreases gradually. The lower the initial coal seam temperature, the more obvious the decrease in permeability. When the extraction time was 3650 days, the permeability ratio with an initial temperature of 300 K decreased by 5.7% compared with the initial coal seam temperature of 340 K. The lower the initial temperature, the smaller the permeability ratio change. This is because as the temperature decreases, the coal seam will have a shrinking effect, and the gas pressure will also decrease, so the permeability rate decline will be slower.

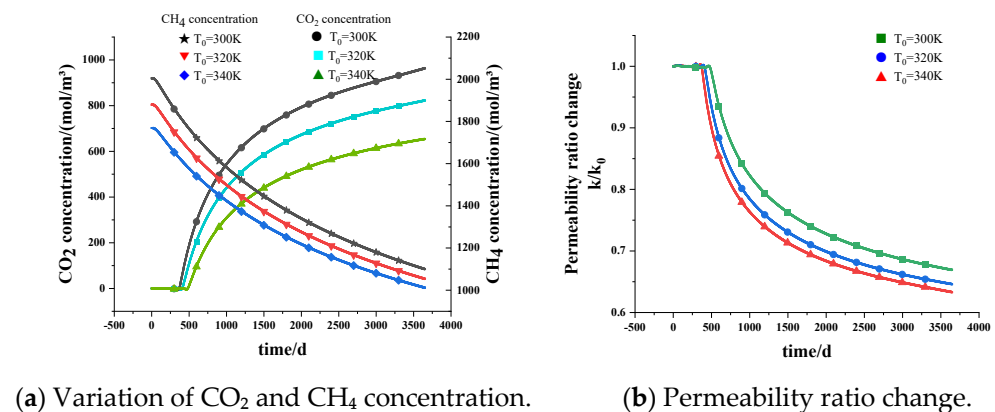


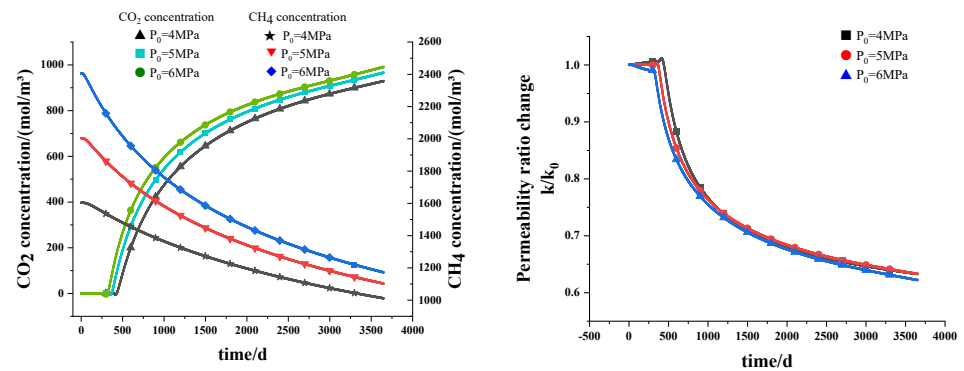
Figure 5. Displacement effect under different initial seam temperatures.

Both CH₄ and CO₂ concentrations decreased with increasing initial coal seam temperature. When the initial coal seam temperature was 300 K, the CO₂ concentration was 966.046 mol/m³ at 3650 days, and the total output of CH₄ was 901.817 mol/m³. When the initial coal seam temperature was 320 K, the CO₂ decreased by 14.6% at 3650 days, and the total output of CH₄ was 822.555 mol/m³, a decrease of 8.8%. When the initial coal seam temperature was 340 K, the CO₂ decreased by 32% in 3650 days, and the total output of CH₄ was 754.145 mol/m³, a decrease of 16.4%. The higher the coal seam temperature, the kinetic energy of injected CO₂ molecules increases, which reduces the adsorption rate of CO₂ to coal [15], the less the gas content in the adsorbed state per unit volume of the coal seam. Therefore, the less total concentration of CH₄ produced. The increase of temperature promotes the desorption and diffusion of binary gas [8]. As the temperature of coal seam increases, the content of adsorbed gas in the coal seam will decrease [1], so the content of CO₂ stored in the coal seam will also decrease.

3.3.2. Displacement Effect under Different Coal Seam Pressures

The displacement effect under different initial coal seam pressures is shown in Figure 6. The concentrations of CH₄ and CO₂ increase with the increase of the initial pressure of the coal seam. When the initial coal seam pressure was 4 MPa, the CO₂ concentration was 929.215 mol/m³ at 3650 days. When the initial coal seam pressure increased to 5 MPa, the CO₂ concentration was 966.046 mol/m³ at 3650 days, an increase of 4%. When the initial coal seam pressure was 6 MPa, the CO₂ concentration was 991.276 mol/m³ at 3650 days, an increase of 6.7%. When the initial pressure was 4 MPa, the total output of CH₄ was 592.085 mol/m³. When the initial coal seam pressure was 5 MPa, the total output of CH₄ was 901.817 mol/m³, an increase of 34.4%. When the initial coal seam pressure was 6 MPa, the total output of CH₄ was 1232.880 mol/m³, an increase of 108.2%. The higher the initial pressure of the coal seam, the higher the initial CH₄ content in the coal seam, and the

higher the concentration of CH₄ production [34]. At the same time, as the initial coal seam pressure increases, the pressure gradient between the coal seam and the CH₄ production well also increases, the seepage velocity increases, and the CH₄ production rate increases. Due to the faster migration of CH₄ in the coal seam, the faster the migration of CO₂ is, and the amount of CO₂ sequestered also increases.



(a) Variation of CO₂ and CH₄ concentration.

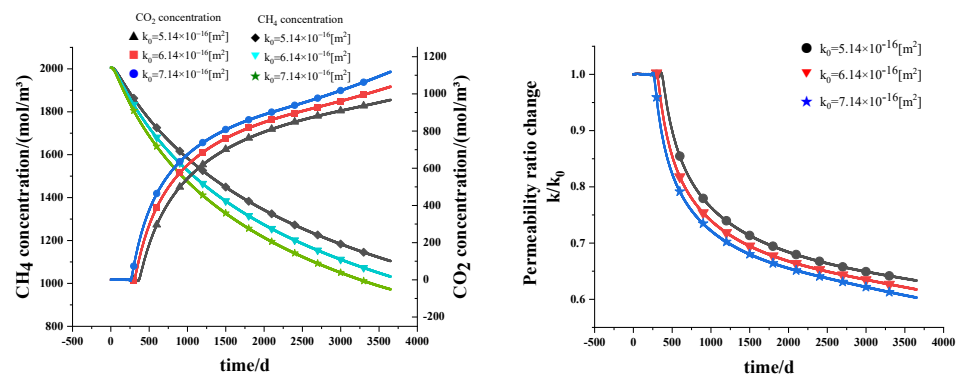
(b) Permeability ratio change.

Figure 6. Displacement effects at different initial coal seam pressures.

The permeability ratio decreases as the initial pressure of the coal seam increases. The increase of the initial pressure of the coal seam will increase the pressure gradient between the CO₂ injection well and the coal seam, promote the acceleration of seepage, reduce the effective stress, reduce the matrix pore radius, and reduce the matrix porosity, so the permeability is also smaller.

3.3.3. Displacement Effect under Different Initial Permeability

The displacement effect under different initial permeability is shown in Figure 7. The greater the initial permeability of the coal seam, the faster the seepage velocity of the binary gas to the production well, the greater the desorption of CH₄ and the adsorption of CO₂, the faster the permeability ratio decreases, and the faster the change [39]. At 3650 days, when the initial coal seam permeability was $5.14 \times 10^{-16} \text{ m}^2$, the permeability ratio increased by 2.5% compared with the condition that the initial coal seam permeability was $6.14 \times 10^{-16} \text{ m}^2$. When the initial coal seam permeability was $7.14 \times 10^{-16} \text{ m}^2$, the permeability ratio is reduced by 4.8% compared with the condition that the initial coal seam permeability was $5.14 \times 10^{-16} \text{ m}^2$.



(a) Variation of CO₂ and CH₄ concentration.

(b) Permeability ratio change.

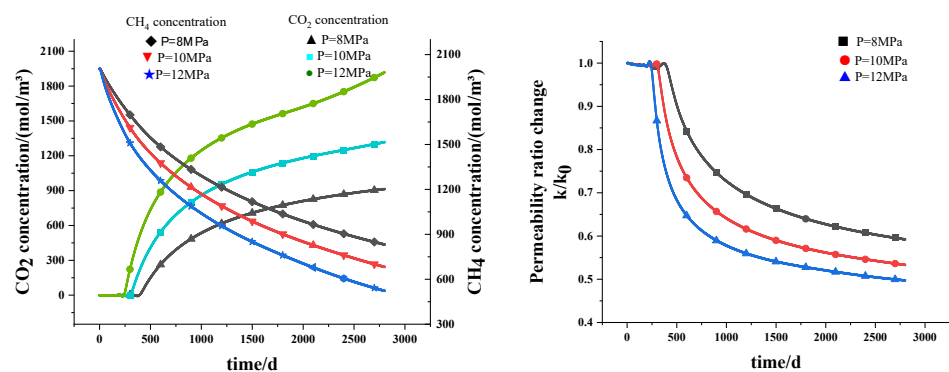
Figure 7. Displacement effects at different initial permeability rates.

It can also be seen from Figure 7 that the displacement effect is better with the increase of the initial permeability. At 3650 days, when the initial coal seam permeability was

$5.14 \times 10^{-16} \text{ m}^2$, the CH_4 storage concentration was 1102.834 mol/m^3 , and the CO_2 storage concentration was 966.046 mol/m^3 . When the initial coal seam permeability increased to $6.14 \times 10^{-16} \text{ m}^2$, the CH_4 storage concentration was 1030.514 mol/m^3 , a decrease of 6.7%, and the CO_2 storage concentration was $1036.94296 \text{ mol/m}^3$, an increase of 7.4%. When the permeability was $7.14 \times 10^{-16} \text{ m}^2$, the CH_4 storage concentration was 971.274 mol/m^3 , a decrease of 11.9%, and the CO_2 storage concentration was $1117.2951 \text{ mol/m}^3$, an increase of 15.7%. In the process of displacement, the greater the initial permeability, the greater the fracture opening of the coal seam, which is more conducive to the seepage and migration of gas [11]. The porosity determines the change of permeability. The larger the initial permeability, the higher the porosity of the coal seam, the more desorption and diffusion paths of CBM. When the initial permeability is relatively small, the matrix gas pressure decreases slowly and the matrix shrinkage effect is not significant [31]. Therefore, a larger initial permeability has a positive effect on increasing the CH_4 output concentration and CO_2 storage concentration.

3.4. Displacement Effect under Different Gas Injection Pressures

The changes of permeability ratio, CH_4 and CO_2 concentrations at point A under different CO_2 injection pressures are shown in Figure 8. The higher the injection pressure, the better the displacement effect at each stage, and the faster the permeability ratio decreases. When the CO_2 injection pressure increased from 8 MPa to 12 MPa, the CH_4 concentration in the coal seam decreased from 831.806 mol/m^3 to 522.494 mol/m^3 at 2800 days, and the CO_2 concentration increased from 914.003 mol/m^3 to 1918.241 mol/m^3 at 2800 days. When the CO_2 injection pressure increased from 8 MPa to 10 MPa, the CH_4 concentration in the coal seam decreased by 149.7933 mol/m^3 at 2800 days, meanwhile the CO_2 concentration increased by 404.260 mol/m^3 at 2800 days. This shows that the increase of CO_2 injection pressure can effectively promote the displacement of CH_4 . The gas pressure gradient will have a great impact on the gas seepage velocity in the coal seam. The larger the CO_2 migration area, the greater the pressure gradient, which effectively increases the CO_2 seepage velocity [40], and this shows that increasing the injection pressure of the injection well can effectively remove the CH_4 in the coal from the original position and improve the effect of displacement [32]. At the same time, increasing the injection pressure will also increase the surface activation energy of the coal, so that the contact and collision opportunities of the binary gas are greater [13], and the adsorption and desorption effect is strengthened, which is conducive to the displacement effect.



(a) Variation of CH_4 and CO_2 concentration.

(b) Permeability ratio change.

Figure 8. Variation of displacement effect under different CO_2 injection pressures.

In the process of CO_2 -ECBM, with the increase of production time, the overall trend showed a decreasing trend, as shown in Figure 8b. The increase of CO_2 injection pressure promotes the larger pressure gradient formed at point A, resulting in a faster decrease in the permeability ratio. Since the CO_2 injection pressure is greater than the initial coal seam pressure, the gas pressure in the coal seam increases, the effective stress decreases,

the matrix pore radius decreases, the matrix porosity decreases, and the permeability decreases [11]. In addition, since the coal seam has a preferential adsorption capacity for CO₂ and the molar amount of adsorbed CO₂ is twice that of CH₄, the injection of CO₂ will cause the coal seam to continuously desorb and adsorb, resulting in the expansion of the coal seam, which further reduces the matrix porosity and permeability. Therefore, under the combined action of injection pressure and competitive adsorption of CO₂ and CH₄, the permeability gradually decreased.

4. Conclusions

A fully coupled coal deformation, binary gas flow and diffusion and gas absorption/desorption finite element model is developed to achieve a better understanding of the CO₂-ECBM recovery mechanisms, and COMSOL Multiphysics was used for numerical simulation. The influence of parameters such as gas pressure, coal seam temperature and permeability on the displacement effect were analyzed. The main conclusions are as follows:

- (1) Under the same working conditions, the increase of the gas injection pressure or the initial coal seam pressure has a positive effect on increasing the cumulative production concentration of CH₄ and the cumulative storage concentration of CO₂.
- (2) With the increase of the coal seam temperature, the CH₄ production concentration and CO₂ storage concentration in the coal seam will decrease, and the permeability ratio will decrease faster.
- (3) In the process of displacement, the greater the initial permeability, the greater the fracture opening of the coal seam, which is more conducive to the seepage migration of gas, and the displacement effect is also better.
- (4) The closer to the injection well, the better the displacement effect and the lower the permeability ratio.

Author Contributions: Supervision, Z.L.; methodology and language correction, Z.L.; numerical simulation, H.Y.; writing and editing, H.Y.; analysis and data correction, Y.B. All authors have read and agreed to the published version of the manuscript.

Funding: This research is financially supported by the National Natural Science Foundation of China (52004176), the Research Project Supported by Shanxi Scholarship Council of China (2022-053) and the Supported by Scientific and Technological Innovation Programs of Higher Education Institutions in Shanxi (2019L0246).

Institutional Review Board Statement: “Not applicable” for studies not involving humans or 258 animals.

Informed Consent Statement: Informed consent was obtained from all subjects involved in the study.

Data Availability Statement: All data included in this study are available upon request by contacting the corresponding author.

Acknowledgments: We are grateful to anonymous reviewers for their constructive reviews on the manuscript, and the editors for carefully revising the manuscript.

Conflicts of Interest: The authors declare that they have no conflict of interest.

References

1. Zhou, Y.; Li, Z.; Zhang, R.; Wang, G.; Yu, H.; Sun, G.; Chen, L. CO₂ injection in coal: Advantages and influences of temperature and pressure. *Fuel* **2019**, *236*, 493–500. [[CrossRef](#)]
2. Long, Y. Experimental study on influence of different rank coal on gas adsorption characteristics and CO₂-ECBM influence. Master's Thesis, China University of Mining and Technology, Beijing, China, 2020.
3. Wolterbeek, T.K.; Peach, C.J.; Raoof, A.; Spiers, C.J. Reactive transport of CO₂-rich fluids in simulated wellbore interfaces: Flow-through experiments on the 1–6m length scale. *Int. J. Greenh. Gas Control* **2016**, *54*, 96–116. [[CrossRef](#)]
4. Raoof, A.; Nick, H.M.; Wolterbeek, T.K.T.; Spiers, C.J. Pore-scale modeling of reactive transport in wellbore cement under CO₂ storage conditions. *Int. J. Greenh. Gas Control* **2012**, *11*, 67–77. [[CrossRef](#)]

5. Liu, Y.; Lebedev, M.; Zhang, Y.; Wang, E.; Li, W.; Liang, J.; Feng, R.; Ma, R. Micro-Cleat and Permeability Evolution of Anisotropic Coal During Directional CO₂ Flooding: An In Situ Micro-CT Study. *Nat. Resour. Res.* **2022**, *31*, 2805–2818. [[CrossRef](#)]
6. Godec, M.; Koperma, G.; Gale, J. CO₂-ECBM: A Review of its Status and Global Potential. *Energy Procedia* **2014**, *63*, 5858–5869. [[CrossRef](#)]
7. Baran, P.; Zarebska, K.; Krzystoliket, P.; Hadro, J.; Nunn, A. CO₂-ECBM and CO₂ Sequestration in Polish Coal Seam—Experimental Study. *J. Min. Sci.* **2014**, *13*, 22–29. [[CrossRef](#)]
8. Gunter, W.D.; Gentzis, T.; Rottenfusser, B.A.; Richardson, R.J.H. Deep coalbed methane in Alberta, Canada: A fuel resource with the potential of zero greenhouse gas emissions. *Energy Convers. Manag.* **1997**, *38*, S217–S222. [[CrossRef](#)]
9. White, C.M.; Smith, D.H.; Jones, K.L.; Goodman, A.L.; Jikich, S.A.; LaCount, R.B.; DuBose, S.B.; Ozdemir, E.; Morsi, B.I.; Schroeder, K.T. Sequestration of Carbon Dioxide in Coal with Enhanced Coalbed Methane Recovery—A Review. *Energy Fuels* **2005**, *19*, 659–724. [[CrossRef](#)]
10. Dutka, B.; Kudasik, M.; Pokryszka, Z.; Skoczylas, N.; Topolnicki, J.; Wierzbicki, M. Balance of CO₂/CH₄ exchange sorption in a coal briquette. *Fuel Process. Technol.* **2013**, *106*, 95–101. [[CrossRef](#)]
11. Talapatra, A. A study on the carbon dioxide injection into coal seam aiming at enhancing coal bed methane (ECBM) recovery. *J. Petrol. Explor. Prod. Technol.* **2020**, *10*, 1965–1981. [[CrossRef](#)]
12. Fang, H.; Sang, S.; Liu, S. Experimental simulation of replacing and displacing CH₄ by injecting supercritical CO₂ and its geological significance. *Int. J. Greenh. Gas Control* **2019**, *81*, 115–125. [[CrossRef](#)]
13. Fang, H.; Sang, S.; Liu, S. Numerical simulation of enhancing coalbed methane recovery by injecting CO₂ with heat injection. *Pet. Sci.* **2019**, *16*, 32–43. [[CrossRef](#)]
14. Fang, H.; Sang, S.; Liu, S. Establishment of dynamic permeability model of coal reservoir and its numerical simulation during the CO₂-ECBM process. *J. Pet. Sci. Eng.* **2019**, *179*, 885–898. [[CrossRef](#)]
15. Qu, H.; Liu, J.; Chen, Z. Complex evolution of coal permeability during CO₂ injection under variable temperatures. *Int. J. Greenh. Gas Control* **2012**, *9*, 281–293. [[CrossRef](#)]
16. Perera, M.S.A.; Ranjith, P.G.; Ranathunga, A.S.; Koay, A.Y.J.; Zhao, J.; Choi, S.K. Optimization of enhanced coal-bed methane recovery using numerical simulation. *J. Geophys. Eng.* **2015**, *12*, 90–107. [[CrossRef](#)]
17. Yang, H.; Wei, C.; Wang, Z.; Yang, T. Numerical simulation of coal-bed methane displacement by underground gas injection based on multi-physics coupling. *J. China Coal Soc.* **2010**, *35*, 109–114.
18. Rutqvist, J.; Wu, Y.S.; Tsang, C.F.; Bodvarsson, G. A modeling approach for analysis of coupled multiphase fluid flow, heat transfer, and deformation in fractured porous rock. *Int. J. Rock Mech. Min. Sci.* **2002**, *39*, 429–442. [[CrossRef](#)]
19. Sun, K. Model and numerical simulation about multispecies fluid diffusion and seepage in exploitation coalbed methane by gas injection. *J. Liaoning Tech. Univ.* **2005**, *24*, 305–308.
20. Li, N. Numerical Simulation Study on CO₂-ECBM and Geosequestration of deep buried area in the Qinshui Basin. Master's Thesis, China University of Mining and Technology, Beijing, China, 2018.
21. Li, S.; Fan, C.; Han, J.; Luo, M.; Yang, Z.; Bi, H. A fully coupled thermal-hydraulic-mechanical model with two-phase flow for coalbed methane extraction. *J. Nat. Gas Sci. Eng.* **2016**, *33*, 324–336. [[CrossRef](#)]
22. Xia, T.; Zhou, F.; Gao, F. Simulation of coal self-heating processes in underground methane-rich coal seams. *Int. J. Coal Geol.* **2015**, *141–142*, 1–12. [[CrossRef](#)]
23. Zhang, H.; Liu, J.; Elsworth, D. How sorption-induced matrix deformation affects gas flow in coal seams: A new FE model. *Int. J. Rock Mech. Min. Sci.* **2008**, *45*, 1226–1236. [[CrossRef](#)]
24. Li, H.; Lin, B.; Yang, W.; Hong, Y.; Wang, Z. A fully coupled electromagnetic-thermal-mechanical model for coalbed methane extraction with microwave heating. *J. Nat. Gas Sci. Eng.* **2017**, *46*, 830–844. [[CrossRef](#)]
25. Guo, H.; Yu, Z.; Zhang, H. Phylogenetic diversity of microbial communities as associated with coalbed methane gas from Eastern Ordos Basin, China. *Int. J. Coal Geol.* **2015**, *150–151*, 120–126. [[CrossRef](#)]
26. Gruskiewicz, M.S.; Naney, M.T.; Blencoe, J.G.; Cole, D.R.; Pashin, J.C.; Carroll, R.E. Adsorption kinetics of CO₂, CH₄, and their equimolar mixture on coal from the Black Warrior Basin, West-Central Alabama. *Int. J. Coal Geol.* **2019**, *77*, 23–33. [[CrossRef](#)]
27. Chen, Z.; Liu, J.; Elsworth, D.; Connell, L.D.; Pan, Z. Impact of CO₂ injection and differential deformation on CO₂ injectivity under in-situ stress conditions. *Int. J. Coal Geol.* **2010**, *81*, 97–108. [[CrossRef](#)]
28. Deng, C.; Fan, Y.; Zhang, X. Numerical Simulation of Fluid-Solid-Heat Coupling for CO₂ Sequestration in Coal Seams. *J. Eng. Thermophys.* **2019**, *40*, 2879–2886.
29. Fan, Y.; Deng, C.; Zhang, X.; Li, F.; Wang, X.; Qiao, L. Numerical study of CO₂-enhanced coalbed methane recovery. *Int. J. Greenh. Gas Control* **2018**, *76*, 12–23. [[CrossRef](#)]
30. Liu, J.; Chen, Z.; Elsworth, D.; Qu, H.; Chen, D. Interactions of multiple processes during CBM extraction: A critical review. *Int. J. Coal Geol.* **2011**, *87*, 175–189. [[CrossRef](#)]
31. Liu, T.; Lin, B.; Yang, W.; Liu, T.; Kong, J.; Huang, Z.; Wang, R.; Zhao, Y. Dynamic diffusion-based multifield coupling model for gas drainage. *J. Nat. Gas Sci. Eng.* **2017**, *44*, 233–249. [[CrossRef](#)]
32. Fang, H.; Sang, S.; Liu, S. The coupling mechanism of the thermal-hydraulic-mechanical fields in CH₄-bearing coal and its application in the CO₂-enhanced coalbed methane recovery. *J. Pet. Sci. Eng.* **2019**, *181*, 106177. [[CrossRef](#)]
33. Pan, Z.; Connell, L.D. Comparison of adsorption models in reservoir simulation of enhanced coalbed methane recovery and CO₂ sequestration in coal, International Journal of Greenhouse Gas Control. *Int. J. Greenh. Gas Control* **2009**, *3*, 77–89. [[CrossRef](#)]

34. Fan, Y.; Huo, Z.; Wang, Y. Numerical simulation of CO₂-ECBM based on fluid-solid-thermal coupling. *Saf. Coal Mines* **2022**, *53*, 162–169.
35. Shi, J.Q.; Mazumde, S.; Wolf, K.H.; Durucan, S. Competitive methane desorption by supercritical CO₂ injection in coal. *Transp. Porous Media* **2008**, *75*, 35–54. [[CrossRef](#)]
36. Connell, L.D. Coupled flow and geomechanical processes during gas production from coal seams. *Int. J. Coal Geol.* **2009**, *79*, 18–28. [[CrossRef](#)]
37. Tao, Y. Study on the gassy coal THM coupling model and coal and gas outburst simulation. Ph.D. Thesis, Chongqing University, Chongqing, China, 2009.
38. Kong, X.; Wang, E.; Liu, Q.; Li, Z.; Li, D.; Cao, Z.; Niu, Y. Dynamic permeability and porosity evolution of coal seam rich in CBM based on the flow-solid coupling theory. *J. Nat. Gas Sci. Eng.* **2017**, *40*, 61–71. [[CrossRef](#)]
39. Fan, C.; Elsworth, D.; Li, S.; Zhou, L.; Yang, Z.; Song, Y. Thermo-hydro-mechanical-chemical couplings controlling CH₄ production and CO₂ sequestration in enhanced coalbed methane recovery. *Energy* **2019**, *173*, 1054–1077. [[CrossRef](#)]
40. Liu, S.; Fang, H.; Sang, S.; Ashutosh, T.; Wu, J.; Zhang, S.; Zhang, B. CO₂ injectability and CH₄ recovery of the engineering test in qinshui Basin, China based on numerical simulation. *Int. J. Greenh. Gas Control* **2020**, *95*, 1750–5836. [[CrossRef](#)]